Large-scale behavior of energy spectra of the quantum random antiferromagnetic Ising chain with mixed transverse and longitudinal fields

Richard Berkovits ⬭

Department of Physics, Jack and Pearl Resnick Institute, Bar-Ilan University, Ramat-Gan 52900, Israel

In recent years, it became clear that the metallic regime of systems that exhibit a many-body localization (MBL) behavior shows properties that are quite different than the vanilla metallic region of the single-particle Anderson regime. Here we show that the large-scale energy spectrum of a canonical microscopical model featuring MBL displays a nonuniversal behavior at intermediate scales, which is distinct from the deviation from universality seen in the single-particle Anderson regime. The crucial step in revealing this behavior is a global unfolding of the spectrum performed using the singular value decomposition (SVD) which takes into account the sample to sample fluctuations of the spectra. The spectrum properties may be observed directly in the singular value amplitudes via the scree plot, or by using the SVD to unfold the spectra and then perform a number of states variance calculation. Both methods reveal an intermediate scale of energies that follow super-Poissonian statistics.

I. INTRODUCTION

Many-body localization (MBL) [1,2] has captured the imagination of researchers since its inception more than a decade and a half ago. Once interactions are introduced to a many-particle system for which all single-particle states are localized, a parameter region where the many-particle states are extended should appear, as expected from the many-body thermalization hypothesis [3,4]. Other regions of the parameter space remain localized even in the presence of interactions. Almost immediately, an effort to identify the transition point by analyzing the spectra of microscopic models of disordered interacting many-particle systems began. The spectra of 1D spin chains and electronic models [5–9] were probed in order to identify a signature of a transition (or crossover) between the two regions. Nevertheless, despite much effort a definitive answer remains elusive.

For microscopic models of MBL, one runs into an insurmountable obstacle in analyzing the energy spectra. The Hilbert space grows exponentially and for conventional computers it is hard to imagine that one will reach large enough systems for which the analysis of the spectra will give an indisputable finite size scaling. Nevertheless, there is still a point in looking into the spectral properties of small microscopic models, for two main reasons. The first, is that although the systems studied are small, there are nevertheless some behaviors that emerge in a robust form even for these sizes. Although it might not be possible to prove that these behaviors survive in the thermodynamical limit, it is still worthwhile to understand them [10]. Second, many current experimental studies searching for a signature of the MBL [11–15] are performed on systems of similar small size.

Here we would like to examine a particular microscopical model of a quantum random antiferromagnetic Ising chain

with mixed transverse and longitudinal fields, sometimes referred in the MBL literature as the Imbrie model. The ground state of this model has been known to exhibit a rich phase diagram [16–18], and recently the model has garnered considerable interest in the context of MBL [19–24]. This interest stems from the assertion that under some assumptions, it is possible to rigorously show that it undergoes a MBL transition from metallic to localized behavior as disorder increases [20].

What is the nature of the extended region of the Imbrie model? Is this region analogues to the single-particle Anderson metallic phase? These are the questions we would like to address in this paper. For single-particle Anderson metallic regime, the energy spectrum follows the random matrix predictions [25–30] up to an energy scale known as the Thouless energy [31], above which a different behavior is observed, where the Thouless energy $E_{\mathrm{Th}} = \hbar D/L^2 = g\delta$ (D is the diffusion constant, L, is the linear dimension, g is the dimensionless conductance, and δ the average level spacing). The physical origin of the Thouless energy is the time needed for a wave packet to cover the whole sample known as the Thouless time $t_{\mathrm{Th}} = \hbar/E_{\mathrm{Th}} = L^2/D$. At shorter times (larger energy scales), the system is not ergodic, hence the different energy spectrum behavior at this scale.

The generalized Rosenzweig-Porter random matrix model (GRP) [32,33] is probably the simplest random matrix model which shows three distinct phases: localized at strong disorder, nonergodic extended (NEE) phase for intermediate disorder, and a fully ergodic extended phase at weak disorder. The NEE phase exhibits unusual features such as fractality of the wave functions [33–40] and super-Poissonian behavior of the energy spectrum at intermediate energy scales [39,41]. Focusing on the energy spectrum, one discovers that the nearest neighbor statistics (small energy scale, corresponding to long times) is indistinguishable from the extended metallic phase,

while for intermediate energy scales a super-Poissonian behavior of the nth level spacing distribution has been observed [39]. Examining the singular value decomposition (SVD) of the spectrum of an ensemble of realizations supports this conclusion. Moreover, the SVD amplitude scree plot, which in the NEE phase show three different regimes as a function of the mode number (essentially inverse energy, where low modes correspond to large energy scales). High modes (small energy scales) show a Wigner behavior, then it crosses to a super-Poissonian behavior for the intermediate range of modes, finally switching at low modes (large energy scales) to a Poisson form [41]. Thus two transition energies in the spectrum emerge. The lower transition energy corresponds to a transition from a universal Wigner behavior typical to the metallic regime, to a nonuniversal NEE regime. Following previous works [42], the energy at which this transition occurs will be termed the Thouless energy. It is important though to note that although the same terminology for the Thouless energy as for the single-particle Anderson transition is used, it does not necessarily mean that the same physics is behind it. This will be discussed further on. The second transition between the NEE regime and Poisson like behavior has no direct analog in the single-particle metallic systems. One must keep in mind that for any system the energy spectrum on large scales is determined by the global band structure which is captured in the first few modes in the scree plot. The NEE behavior has an additional timescale which is the onset of the extended behavior. Thus a region of small modes of the SVD will be needed to capture the pre-extended region. The energy for which the extended behavior is manifested is the second transition energy and will be termed, E_{Ex}, the extended energy. Much of the interest in the GRP model stems from the proposal that it might capture properties relevant to MBL systems. Indeed we will demonstrate that these two transition energies emerge also for the Imbrie model, and the meaning of this large energy scale will be discussed further on.

One of the most interesting questions investigated by the MBL community [21,43–54] is the nature of the metallic regime close to the localized regime. This region exhibits at intermediate times (intermediate energy scales) different behavior than expected from the canonical Anderson transition. For example, the time evolution of the system is sub-diffusive and relaxation toward equilibrium is anomalously slow [55–63], a behavior that might have been seen also in experiments [11,64,65]. The same region also exhibits fractal behavior of the eigenfunctions [24].

The fractal behavior of the eigenfunctions as well as the subdiffusive time evolution have several complementary explanations. One of the main routes to an explanation of the NEE behavior is via the picture localization in the Fock space, which has originally motivated the study of MBL [2,66]. Essentially the coupling of states in the Fock space creates a quantum random graph which leads to nonergodic behavior and fractal structure of the states in Fock space. This behavior has also been associated to rare regions in the 1D systems known as the Griffiths regions [56,61,67–72], which could explain the subdiffusive behavior. Evidence for Griffiths regions in 2D exists [75–78] as well as observations of subdiffusive behavior in numerical [73,74] and experimental many-body systems [65]. It is interesting to see whether subdiffusive

behavior is seen for higher dimensions for which Griffiths regions are more unlikely. A complementary view suggests that the MBL transition is a Kosterlitz Thouless (KT) transition [24,79–83]. In this picture, rare regions of extended states may appear which will lead to an avalanche delocalizing the whole sample if disorder is not too strong. This will lead naturally to fractal structure of the Hilbert space and to a NEE behavior.

Here we would explore whether there are signatures of super-Poissonian statistics at intermediate energies in the Imbrie model, similar to the behavior seen in GRP. The usual way of examining the behavior at large energy scales is the variance of the number of levels as function of the size of an energy window after a local unfolding of the energy spectrum, i.e., $\langle \delta^2 n(E) \rangle = \langle (n(E) - \langle n(E) \rangle)^2 \rangle$, where $\langle \ldots \rangle$ denotes an average over an ensemble of different realizations of disorder and $n(E)$ is the number of levels within an energy window E. In the Poisson regime $\langle \delta^2 n(E) \rangle \sim \langle n(E) \rangle$, while in the Wigner regime it grows logarithmic. Deviation from the logarithmic behavior to a stronger than linear behavior at large energies have been seen in metallic system beyond the Thouless energy [84,85], the Sachdev-Ye-Kitaev (SYK) model [42,86], and many-body localization systems [87–89]. Essentially, local unfolding assumes that the density of states is smooth and similar for different realizations of disorder in the ensemble and therefore the average level spacing may be calculated by an average over a narrow window of energy (usualy O(10) levels) over the disorder ensemble. As we have shown in Refs. [41,93] there are some problems in the application of the local unfolding in systems where the local density shows strong sample to sample fluctuations or a nonsmooth band structure with long range correlations which may skew the results. Therefore, a global unfolding method, which can filter out these long range, realization specific, properties of the spectra at shorter energy scales should be used.

In order to circumvent these problems we will use a different method to study the properties of the spectra, known as singular value decomposition (SVD). This method has been successfully applied to analyze the transition from Wigner to Poisson statistics in the Anderson transition [90–92], to characterizing the NEE in the GRP model [41], to study the large energy scale spectrum behavior beyond the Thouless energy in metallic systems [93], and very recently to the MBL transition in the Heisenberg chain [94].

As will be discussed in detail in the Appendix, SVD essentially returns a set of modes which can be used to construct the energy spectra of the different realizations in the ensemble. Arranging the modes according to the size of their amplitude squared, λ_k (where $k = 1$ is the largest), the first few λ_k ($O(1)$) correspond to global features of the spectra [41,90–92]. Thus one can globally unfold the spectra by filtering out these modes when reconstructing the spectrum. Then the unfolded spectrum can be used to obtain the number variance. A different way to obtain a comprehensive picture of the behavior of the energy spectrum is to plot λ_k versus k, also known as a scree plot. Usually, a power-law behavior $\lambda \sim k^{-\alpha}$, is detected for certain ranges of k. The power-law exponent corresponds to the statistics of the energy spectrum with $\alpha = 2$ for the Poisson behavior, $\alpha = 1$ for the Wigner regime [41,90–92]. For energies larger than E_{Th} (small values of k) in the metallic regime of a single-particle Anderson model $\alpha = 1 + d/2$

(where d is the dimensionality) [93]. In Ref. [41], we have shown that for GRP model in the NEE phase shows for intermediate values of k a power-law behavior with $\alpha > 2$. This behavior is consistent with super-Poissonian statistics. At large values of k (short energy scales) $\alpha = 1$ as expected in the Wigner regime. At small values of k, the singular value curve returns to the $\alpha = 2$ exponent, i.e., Poisson statistics. Thus the super-Poissonian behavior starts at the Thouless energy, and terminates at E_{Ex}. Moreover, as has been discussed in Ref. [93], the power law of the SVD amplitude scree plot is connected to the power-law behavior of the number variance, $\langle \delta^2 n(E) \rangle \sim \langle n(E) \rangle^\beta$, with $\beta = \alpha - 1$, where in the Poisson regime $\alpha = 2$ and $\beta = 1$, while in the Wigner regime $\alpha = 1$ and $\beta = 0$ (actually logarithmic). In the NEE regime one expects a super-Poissonian behavior of the number variance $\beta > 1$ and therefore $\alpha > 2$.

In this paper, we shall introduce the random antiferromagnetic Ising chain (Imbrie model) in Sec. II. The dependence of the density of states and ratio statistics (nearest neighbor level statistics) on the strength of disorder is presented in Sec. III. As expected, above a certain strength of disorder finite size scaling indicates a localized regime, while for weaker disorder an extended regime emerges. Then (Sec. IV) the locally unfolded spectra is used to study the level number variance. The results deviate from RMT predictions (whether Wigner in the extended regime or Poissonian the localized) for higher energy scales, and in the extended regime seem to follow a super-Poissonian behavior. Nevertheless, due to the structure of density of states as well as to strong sample to sample fluctuations, one must question the validity of the local unfolding. Therefore we turn to the SVD scree plot, in order to get a better picture of the larger energy scale behavior of the spectrum in Sec. V. The scree plot suggests that for small energies, the system follows the expectations garnered from the ratio statistics. Then at a particular mode (corresponding to the Thouless energy) the power law changes to a super-Poisson value ($\alpha > 2$). For large energies a second transition is seen in the lower modes corresponding to E_{Ex}, which switches the power lat back to $\alpha \sim 1$. Thus an intermediate range of energies with super-Poissonian statistics emerges for the extended side of the Imbrie model. For the localized regime, no super-Poissonian regime exists and the Poisson exponent transits into a smaller exponent $\alpha < 2$ for low modes. This transition mitigates as one moves deeper into the localized regime. In Sec. VI, SVD is used to globally unfold the spectra and investigate the globally unfolded level number variance, resulting in values of β that correspond well with the α deduced from the scree plot. These results as well as further ramifications are discussed in Sec. VII.

II. IMBRIE MODEL

The Hamiltonian for the random antiferromagnetic Ising chain of length L with mixed transverse and longitudinal fields (Imbrie model) is given by [19–23]

$$\hat{H} = \sum_{i=1}^{L} h_i \hat{S}_i^z + \sum_{i=1}^{L} \gamma_i \hat{S}_i^x + \sum_{i}^{L-1} J_i \hat{S}_i^z \hat{S}_{i+1}^z, \qquad (1)$$
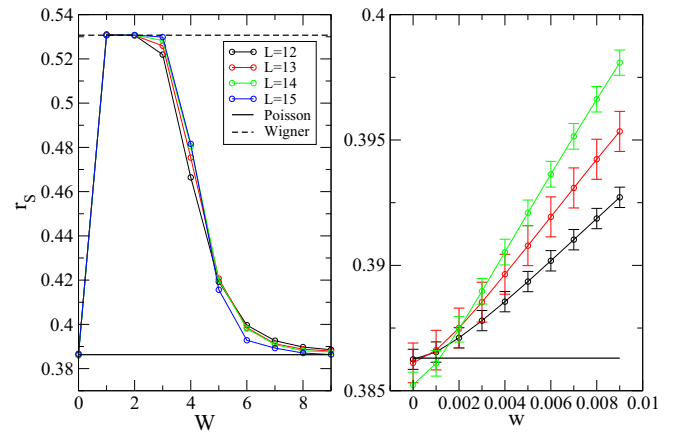

FIG. 1. The ratio statistics r_s [Eq. (2)] as a function of the disorder W, for different system sizes $L = 12, 13, 14,$ and 15. Averaging was performed over 3000 realizations for $L = 12, 13,$ and 14, while for $L = 15$, the averaging was performed over 1000 realization. Circles correspond to the numerical results, while the r_s values for Wigner GOE and Poisson are indicated by continuous and dashed lines. On the left side the whole range of W is presented while on the right side a zoom into small values of W (for $L = 12, 13,$ and 14) is shown.

where S_i^a is the spin on site i in direction $\hat{a}$. h_i is a random magnetic field in the $\hat{z}$ direction on site i drawn from a box distribution between $-W/2$ and $W/2$, and $\gamma_i = 1$. J_i are the nearest-neighbor spin-spin antiferromagnetic interactions which following Abanin *et al.* [23] are drawn from a box distribution in the range 0.8 and 1.2. L is the length of the chain.

The corresponding to Hilbert space has size of 2^L, and we calculate the eigenvalues E_i using exact diagonalization for M realizations for a given disorder.

III. SMALL-ENERGY SCALES

As a first step, we would like to calculate the nearest neighbor level spacing statistics in order to establish for which values of disorder W we see extended states. Since small energy scales for the extended regime follow the Wigner statistics while for the localized regime they follow Poisson statistics, a finite size scaling of a measure probing the nearest neighbor level statistics should reveal in what regime the system is. As a measure we shall use the ratio statistics [5], defined as

$$r = \left\langle \min\left(r_n, r_n^{-1}\right) \right\rangle,$$
$$r_n = \frac{E_n - E_{n-1}}{E_{n+1} - E_n}, \qquad (2)$$

where E_n is the nth eigenvalue of the Hamiltonian and $\langle \ldots \rangle$ is an average over different realizations of disorder and a range of eigenvalues around the middle of the energy spectrum. This measure has the advantage of avoiding the unfolding procedure. For the Poisson statistics, $r_s = 2 \ln 2 - 1 \cong 0.3863$, while for the GOE Wigner distribution, $r_s \cong 0.5307$ [95].

In Fig. 1, r_s, for sample sizes, $L = 12, 13, 14,$ and 15 (corresponding to Hilbert space sizes of 2^L), is presented.
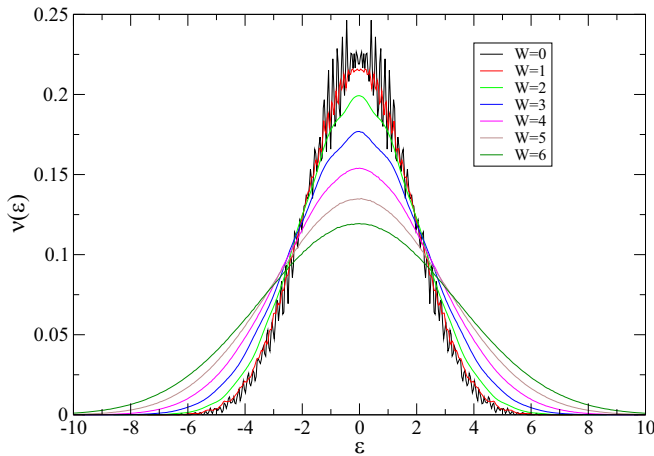
FIG. 2. The density of states $\langle \nu(\varepsilon) \rangle$ as a function of the energy ε for $L = 14$ and different values of disorder averaged over $M = 3000$ different realizations of disorder.

FIG. 3. The averaged level spacing $\delta_p(l)$ as a function of p the level at the center of the range l over which the average is calculated for a *single* realization with different values of l. Two typical realizations of size $L = 14$ and $W = 2$ are presented.

The matrices were exactly diagonalized and all eigenvalues E_n were obtained. r_s was averaged over M realizations, where $M = 3000$ for $L = 12$, 13, and 14, while for $L = 15$, $M = 1000$ realizations, using $P = 2^L/2$ eigenvalues around the center of the band. For finite W a typical transition pattern is seen: above $W \sim 5$ the larger is L the lower the value of r_s and the closer to the Poisson value it becomes. Below the value of $W \sim 5$ (except for in the vicinity of $W = 0$) the order is the opposite, the larger the L, the higher its r_s value is and closer its value is to the GOE statistics. All the curves seem to cross at the same value of $W \sim 5$. Thus, roughly speaking, the behavior of r_s shows the finite size scaling features of a second order localization transition. At $W = 0$, the system again coalesces at the Poisson value. As can be seen from the right panel the finite size behavior indicates that the crossover occurs very close to $W = 0$.

Since our aim in this study was to investigate the extended regime and not to determine the nature of the transition to the localized regime, the values of W around the intersection of the curves was not calculated with enough points around it and the averaging was not performed on a sufficient large number of realization to establish that the crossing corresponds to a second order transition. At this point, we can not be sure that the crossing does not drift with size or show Kosterlitz-Thouless like behavior.

IV. NUMBER VARIANCE WITH LOCAL UNFOLDING

We start by plotting the average density of states $\nu(\varepsilon)$ for different values of disorder. As can be seen in Fig. 2 the level density widens as expected when the disorder increases. Moreover, it is also apparent that the density becomes more smooth as W increases. For $W < 2$ some additional (quasi) regular structure of the density is seen.

Even for stronger disorder where the average density of states seems smooth, significant realization dependent structure remain. This can bee seen in Fig. 3 where the averaged level spacing over a range of eigenvalues l around the p-th level $\delta_l(p) = (E_{p+l/2} - E_{p-l/2})/l$ is plotted. Two typical realizations are presented for $W = 2$, where p ranges over the the
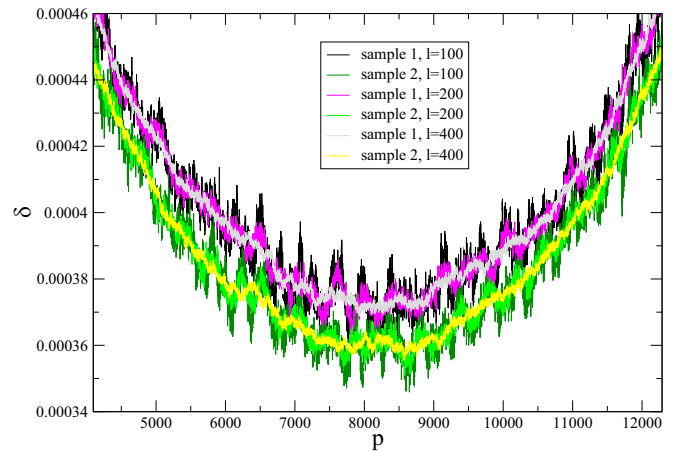
middle half of the eigenvalues, while three different values of $l = 100$, 200, and 400 are presented. In addition to the expected smooth global increase of δ as p moves from the center of the band, $\delta_p(l)$ shows long range sample specific fluctuations on scales of hundreds of levels.

Such a behavior hints towards the existence of a large-scale structure of the energy spectrum and sample to sample fluctuations. This poses a challenge since when one studies the number variance one would like to filter out global or sample dependence regular behavior. This can be problematic since one has to separate global behavior from sample to sample fluctuations. Let us start by a naive application of the local unfolding. In order to calculate $\langle \delta^2 n(E) \rangle$, we unfold the spectrum by $\varepsilon_i = \varepsilon_{i-1} + 2m(E_i - E_{i-1})/\langle E_{i+m} - E_{i-m} \rangle$ where $m = 6$ (other values were used with no significant change). We place the window at the center of the band then the averages $\langle n(E) \rangle$ and $\langle n^2(E) \rangle$ are calculated over all M realizations. The results are shown in Fig. 4

The variance $\langle \delta^2 n(E) \rangle$ as a function of $\langle n(E) \rangle$ is depicted in Fig. 4 for $L = 14$ (matrix linear size $2^{14} = 16384$) and two values of disorder $W = 0$ and 2. As we have seen from the ratio statistics r_s (Fig. 1), $W = 0$ follows Poisson statistics for small energy scales while $W = 2$ follows Wigner at these scales. Indeed, as can be seen in the inset of Fig. 4, for small values of $\langle n \rangle$ the expected behavior of the number variance is followed, i.e., $\langle \delta^2 n(E) \rangle = \langle n \rangle$ for Poisson and $\langle \delta^2 n(E) \rangle = (2/\pi^2) \ln(\langle n(E) \rangle) + 0.44$ for Wigner (GOE). Nevertheless, as larger energies are examined, strong deviations from the Poisson or Wigner behavior are observed.

The large-scale behavior is very different between these two values of disorder. For $W = 0$, the linear behavior quickly saturates, but a very nonmonotonous behavior is apparent. One cannot escape the feeling that a large-scale structure with strong sample to sample fluctuation that lurks in the spectra is not correctly addressed by the local unfolding. For $W = 2$ the large-scale behavior is quite monotonous, shows a strong super-Poissonian behavior where the the number variance shows a power-law dependence on the average number of states, $\langle \delta^2 n(E) \rangle \sim \langle n \rangle^\beta$ with $\beta = 2.02 \gg 1$. Although the fit
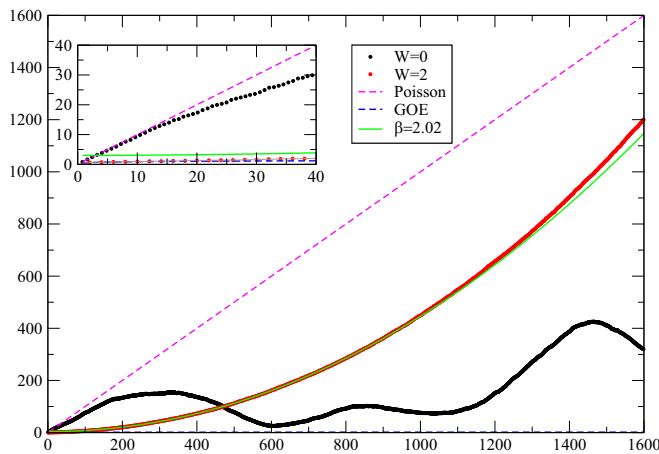
FIG. 4. The variance $\langle \delta^2 n(E) \rangle$ as a function of $\langle n(E) \rangle$ for $L = 14$ with disorder $W = 0$ and $W = 2$. The Poisson behavior, $\langle \delta^2 n(E) \rangle = \langle n(E) \rangle$, and Wigner behavior, $\langle \delta^2 n(E) \rangle = (2/\pi^2) \ln(\langle n(E) \rangle) + 0.44$, are indicated by dashed curves. The inset zooms into the small n region, where the expected Poisson (for $W = 0$) and Wigner ($W = 2$) behavior is seen. For larger energy scales depicted in the main figure, a completely different behavior is seen. For $W = 0$, a very nonmonotonous behavior is observed, while for $W = 2$, $\langle \delta^2 n(E) \rangle \sim \langle n(E) \rangle^\beta$ with $\beta = 2.02$ fits reasonably well.

seems rather decent, one must wonder how reliable is it and whether we are seeing an artifact of the local unfolding.

A possible cure to the sample to sample fluctuations is averaging also over the center of the energy window. In Fig. 5, the number variance is also averaged over 21 positions of the center of the energy window, $\tilde{E}$, equally spaced around the band center, where the furthest point is no more than $1/15$ of the bandwidth from the center. The number of states, $n(E, \tilde{E})$, in a window of width E centered at $\tilde{E}$, is calculated, then the averages $\langle n(E) \rangle$ and $\langle n^2(E) \rangle$ are taken over all positions of the center $\tilde{E}$ and all M realizations. As can be seen, the large scale nonmonotonous behavior for $W = 0$ is somewhat dampened,
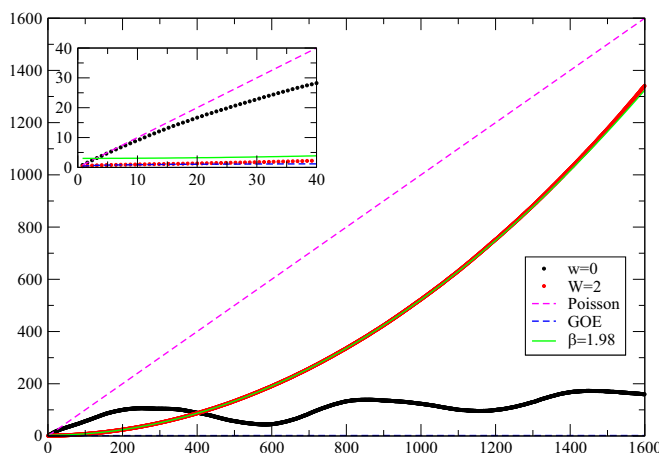

FIG. 5. As for Fig. 4, with an additional average over different positions of the center of the energy window. The averaging does not change much. For the large energy scales in the localized case ($W = 0$), the nonmonotonous behavior is somewhat dampened, while for $W = 2$, $\beta = 1.98$ is similar to the previous result.

while the behavior for $W = 2$ remains essentially the same. Nevertheless, the question remains how much of these results are an artifact of the unfolding and sample to sample fluctuations. We shall address global methods of unfolding in the next sections.

V. SINGULAR VALUE DECOMPOSITION SCREE PLOT

As result of these difficulties with the local unfolding, we change tack and use a different method to study the spectrum, i.e., the SVD method. In this method, no local unfolding is performed, and is replaced by global unfolding. Essentially the spectrum of M realizations of disorder each with P eigenvalues is arranged as a matrix X of size $M \times P$ where X_{mp} is the p level of the mth realization. As detailed in the Appendix after carrying out SVD on X, we can write the matrix as a sum of amplitudes, σ_k, multiplied by matrices, $X^{(k)}$, i.e., $X = \sum_k \sigma_k X^{(k)}$. One may rank the amplitudes from the largest to the smallest, and thus the lower values of k represent modes with higher contributions to reconstructing the matrix. Moreover, the lower modes tend to code the global behavior of the matrix. Plotting the singular values squared $\lambda_k = \sigma_k^2$ according to their rank is knows as the singular value scree plot [96–98] and much information can be gleaned from it. This approach has been applied to the spectrum of disordered systems in several studies [41,90–93], the first few λ_k ($k \leqslant O(1)$) correspond to global features of the spectra. Higher SV (λ_k) show a power-law behavior $k^{-\alpha}$. In the Poisson regime $\alpha = 2$ for high modes, while $\alpha = 1$ in the Wigner regime.

For the GRP model [41], the same behavior was seen for weakly disordered (extended) and strongly disordered (localized) regime. For the intermediate disorder NEE regime, one expects small energy scales to show Wigner properties. Indeed, large k's follow $\alpha \sim 1$. Intermediate values of k, corresponding to intermediate energy scales show unconventional behavior. They follow a power law, but with $\alpha > 2$. This super-Poissonian behavior was interpreted as the signature of the NEE phase. At small k corresponding to larger energy scales (small times), a return to an exponent of $\alpha = 2$ is observed.

A somewhat similar picture emerges for the Imbrie model. Increasing the disorder results in a change of the dependence of the SV amplitudes on the mode number k. For $W = 0$, the high k values follow a power law $\lambda_k \sim k^{-\alpha}$ with $\alpha = 2$, as expected from a localized system, matching with ratio statistics results (Fig. 6). A sudden switch in the exponent to $\alpha = 1$ occurs at $k \sim 200$. This exponent is equal to the exponent exhibited by Wigner statistics.

As can be seen in Fig. 6, for weak disorder ($W = 1, 2$), the behavior of the SV is quite different. For $k > 200$ and $W = 1, 2$ an exponent of $\alpha = 1$ is evident, as expected from systems in the Wigner (extended) regime. This changes to an exponent larger than two (for $W = 1$, $\alpha = 2.3$ for $95 < k < 150$; for $W = 2$, $\alpha = 2.3$ for $40 < k < 105$) for intermediate values of k. Then, similarly to $W = 0$, the exponent switches back to $\alpha = 1$. Thus, in the regime of extended behavior, the SV amplitudes have three distinct behaviors for different ranges of k. Wigner for large values of k (small energy scales, long times), super-Poissonian ($\alpha > 2$) for an intermediate range of k, and back to $\alpha = 1$. This indicates that the extended
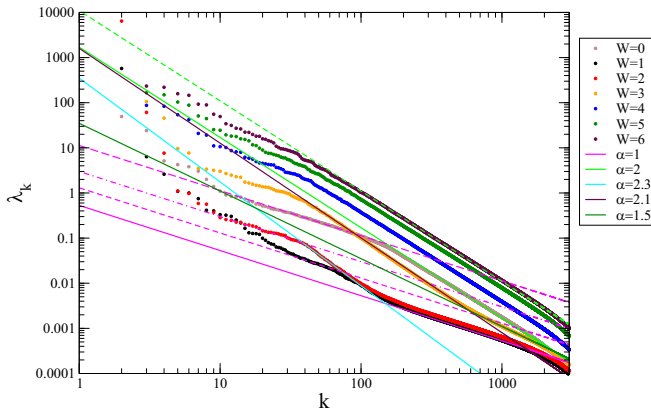
FIG. 6. The scree plot of the singular value amplitudes squared λ_k, where k is the rank of the amplitude from highest to lowest, for $L = 14$ and different values of disorder W. $P = L^2/2 = 8192$ eigenvalues were taken from the middle of the band for $M = 3000$ realizations. Fits to power laws $\lambda_k \sim k^{-\alpha}$, are depicted by the lines, where the magenta lines correspond to $\alpha = 1$, the green lines to $\alpha = 2$, cyan to $\alpha = 2.3$, maroon to $\alpha = 2.1$, and dark green to $\alpha = 1.5$.

FIG. 7. The scree plot of λ_k, as a function of k for $L = 14$ and $W = 2$ with $P = 2^L/2 = 8192$ eigenvalues around the center of the band. Different number of realizations, $M = 1000, 2000, 4000, 6000$, are presented in the inset. In the main plot we scale the different SV amplitudes by dividing λ_k by M. Fits to a power laws, $\lambda_k \sim k^{-\alpha}$, are depicted by the lines, where the magenta line correspond to $\alpha = 1$, and the cyan to $\alpha = 2.3$.

regime in the Imbrie model is far from trivial and signatures of different physics show up at intermediate energy scales. This behavior is somewhat similar to the behavior seen for the SV in the GRP model [41]. Both the GRP and Imbrie models in the extended regime exhibit Wigner behavior at large times (small energy scales, large k), super-Poissonian behavior associated with non ergodicity at intermediate times and energy scales. For short times (large energy scales, small k) the Imbrie and the GRP models show a different behavior expressed by different exponents ($\alpha = 2$ for GRP, $\alpha = 1$ for Imbrie). That is the result of the large-scale structure of the density of states seen in Fig. 2, very clearly for $W = 0$, but still hinted for somewhat stronger disorder. We shall elaborate on it in the following section. Thus SVD provides support for the existence of a NEE regime for the Imbrie model in the weakly disordered extended regime.

For $W = 3$, a crossover behavior is seen. For $700 < k < 2000$, $\alpha = 1.5$ while for $50 < k < 700$, $\alpha = 2.1$, and then for $10 < k < 30$, $\alpha = 1$. Clearly, even for large k we do not see a clear GOE behavior expected on the basis of the ratio statistics behavior (Fig. 1). The SV scree plot behavior seems as a crossover between Poisson and Wigner. Thus, although finite size behavior of nearest neighbor ratio statistics unequivocally puts the $W = 3$ disorder in the Wigner regime, the larger energy scales do not show it. This indicates that the larger energy scales which correspond to short times are crossing over to a closer to Poisson behavior earlier than the short energy scales. The Wigner regime transits to higher α values, while the NEE regime moves towards smaller values of α closer to two. Indeed, The $W = 4$ shows an almost pure Poisson behavior although the disorder is smaller than the critical disorder associated with the ratio statistics. A similar difference between the ratio statistics corresponding to level spacing scale and scree plot behavior was very recently noted in Ref. [94] for the Heisenberg chain.

In the localized regime ($W = 5$ and 6) the expected Poisson exponent, $\alpha = 2$, is seen for $k > 100$. For smaller values
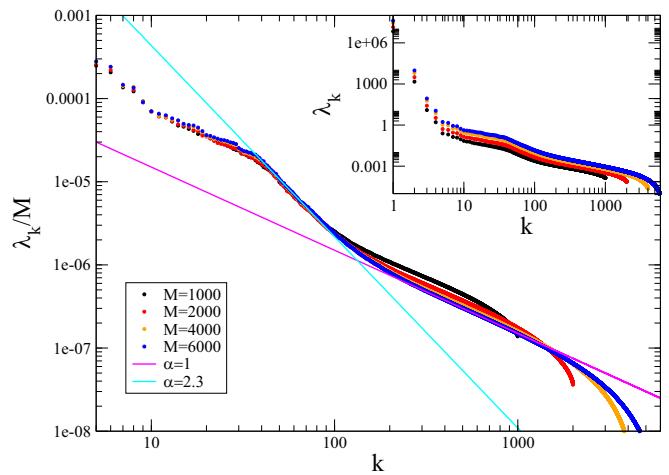
of k, the exponent tappers, and it is hard to determine whether λ_k even follows a power law at all. Nevertheless, it looks that this region becomes smaller as W increases.

Returning to the weakly disordered metallic regime, we would like to examine more carefully the intermediate energy scale for which the super-Poissonian behavior is observed. The first issue to address is the dependence of the scree plot on the number of realizations M. In Fig. 7, λ_k as a function of k for $L = 14$ and $W = 2$ with a range of $P = 2^L/2 = 8192$ eigenvalues around the center of the band are shown. Four different numbers of realizations $M = 1000, 2000, 4000,$ and 6000 have been calculated and are presented in the inset of Fig. 7. As the number of SV modes $r = \min(M, P)$ (see Appendix), and here $P > M$ in all cases, the number of modes is $r = M$. It is clear that for small k's the curves are very similar. Rescaling λ_k to λ_k/M results in all the curves falling on top of each other for $k < 100$ (Fig. 7). In the intermediate regime $40 < k < 100$ for which the super-Poissonian regime with an exponent of $\alpha = 2.3$ is observed the scaled curves coalesce almost perfectly. For higher modes ($k > 100$) although the curves do not coalesce (which is natural since they terminate at different values of $k = M$), nevertheless, the exponents are all $\alpha = 1$ for a significant range of k. Thus, for a reasonable number of realizations, one gets a decent representation of large and intermediate scale behavior of the energy spectrum.

When one increases the range of eigenvalues, P, while keeping the number of realization M fixed it is possible track the two energies determining the crossover from GOE to super-Poissonian behavior, E_{Th}, and the transition from the super-Poissonian regime to a Poissonian regime, E_{Ex}. One might expect that since SVD modes describe the energy spectrum of width $P\delta$, resulting in the kth mode corresponding to a $P\delta/k$ energy range. Thus the position of k_{Th}, the mode for which the exponent changes should depend linearly on P.
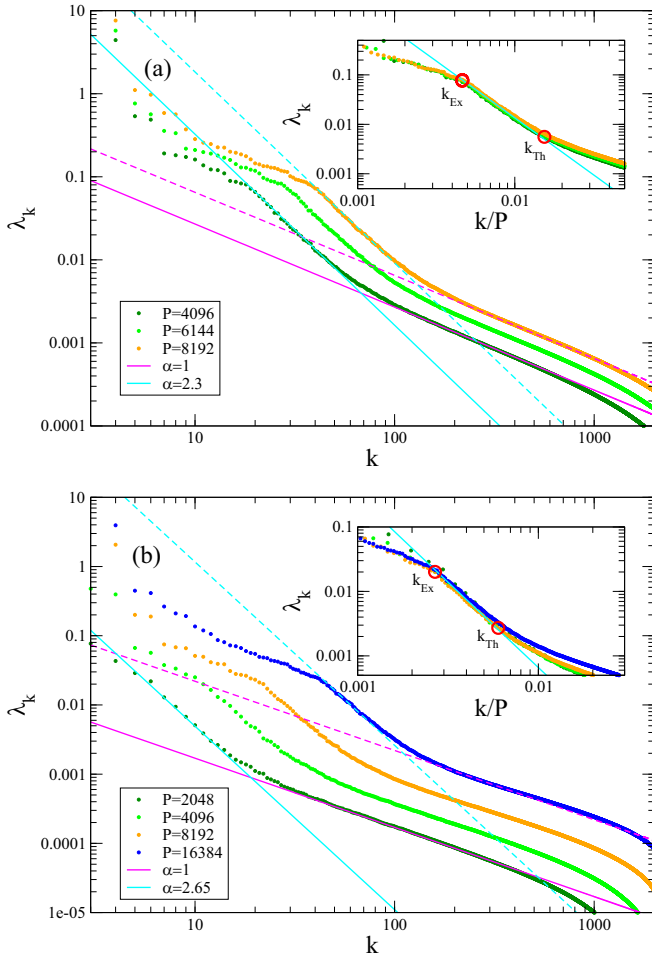
FIG. 8. The scree plot of λ_k, as a function of k for (a) $L = 14$ ($M = 4096$); (b) $L = 15$ ($M = 2048$), in the weak disorder $W = 2$ regime. Different ranges of eigenvalues $P = 4096$, 6144, and 8192 around the center of the band for $L = 14$ and $P = 2048$, 4096, 8192, and 16 384 for $L = 15$ are drawn. Fits to power laws are depicted by the lines, where the magenta lines correspond to $\alpha = 1$, and the cyan to $\alpha = 2.3$ for $L = 14$, while $\alpha = 2.65$ For $L = 15$. (Inset) Zoom into the region intermediate energy scale. Once the SV amplitudes λ_k are scaled by $1/P$, all curves coincide. The red circles indicate the position of the crossover from GOE to super-Poissonian behavior (k_{Th}) and the transition from the super-Poissonian regime back to a Wigner regime (k_{Ex}).

Indeed, from Fig. 8, which presents a scree plot of the SV of $L = 14$ ($2^L = 16\,384$) and $L = 15$ ($2^L = 32\,768$) deep in the weak disorder regime ($W = 2$) for $M = 4096$ ($L = 14$) or $M = 2048$ ($L = 15$) realizations, and different ranges of eigenvalues P centered around the middle of the band, one can see that the SV amplitudes, λ_k, scale as $1/P$. As can be seen in the insets, all curves coincide after rescaling. Estimating the energy scales from the scree plots leads to: $E_{\text{Th}} \sim P\delta/k_{\text{Th}} \sim 80\delta$ ($L = 14$) and $E_{\text{Th}} \sim 160\delta$ ($L = 15$). Similarly, $E_{\text{Ex}} \sim M\delta/k_{\text{Ex}} \sim 200\delta$ ($L = 14$) and $E_{\text{Ex}} \sim P\delta/k_{\text{Ex}} \sim 400\delta$ ($L = 15$). Since, roughly speaking, $\delta \sim B/2^L$, (where B is the band width which depends only weakly on L), one may postulate that E_{Th} and E_{Ex} correspond to a fixed fraction of the band width for the same disorder. The values of E_{Th} and
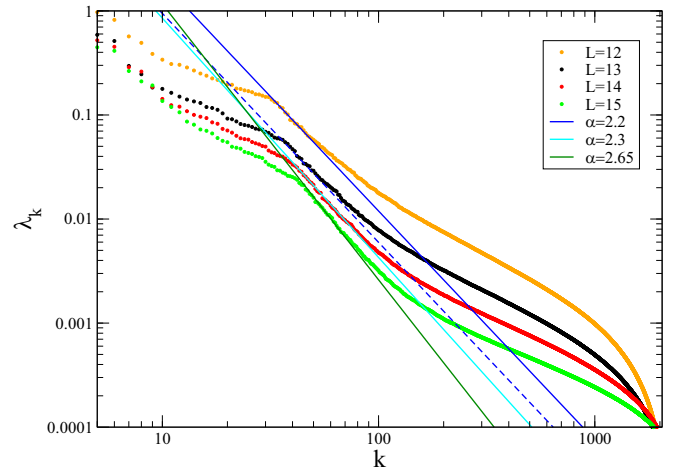

FIG. 9. The scree plot of λ_k, as a function of k for $W = 2$ and four sizes of $L = 12$, 13, 14, and 15 with $M = 2048$ realizations. In all cases, $P = 2^L/2$. Fits to power laws $\lambda_k \sim k^{-\alpha}$, are depicted by the lines, where the blue line correspond to $\alpha = 2.2$ (fit $L = 12$ and 13), the cyan to $\alpha = 2.3$ ($L = 14$), and the dark green to $\alpha = 2.65$ ($L = 15$). The transition between the universal and super-Poissonian behavior, k_{Th}, and between the super-Poissonian and large-scale behavior, k_{Ex}, is similar for all sizes.

E_{Ex} are within the same ranges for which we observed the large-scale structure in Fig. 3.

In Fig. 9, we probe the influence of size, L, on the intermediate region. Here $L = 12$, 13, 14, and 15, $W = 2$ and $M = 2048$ realizations are considered for all sizes. In all cases, $P = 2^L/2$ (half of the eigenvalues around the middle of the band). The exponent in the intermediate energy range increases as the size becomes larger. For $L = 12$ and 13, the exponent $\alpha = 2.2$, for $L = 14$ its $\alpha = 2.3$, and for $L = 15$, the largest size considered here, $\alpha = 2.65$. One may conclude that the intermediate super-Poissonian behavior is enhanced by the increase of the system size. Moreover, the crossover regions between the regions becomes sharper and k_{Th} and k_{Ex} easier to pinpoint as L increase. It can be also seen that for all sizes the Thouless and large-scale energy scales do not vary much, in line with our previous conclusion that they depend on the band width.

Although E_{Th} moves to lower energies as W increases (at least when W approaches the transition value) similar to the Thouless energy for the single-particle Anderson model there are nevertheless important differences for the larger energy scales. Indeed, for both Anderson localization and Imbrie (or GRP), the behavior on larger scales is super-Poissonian ($\alpha > 2$), but there are two main differences. The first is that while for the Anderson case α depends mainly on dimension and only weakly on W and not at all on L, for the Imbrie model the power law has a very strong dependence on disorder and system size. The second difference is that for the Imbrie model an additional energy scale (E_{Ex}) is evident, while for the Anderson model it is absent.

Thus the super-Poissonian regime seems robust and not a fluke of the range of eigenvalues considered or small size. Nevertheless, from the available data it is not possible to extrapolate what is the α value at infinite size.
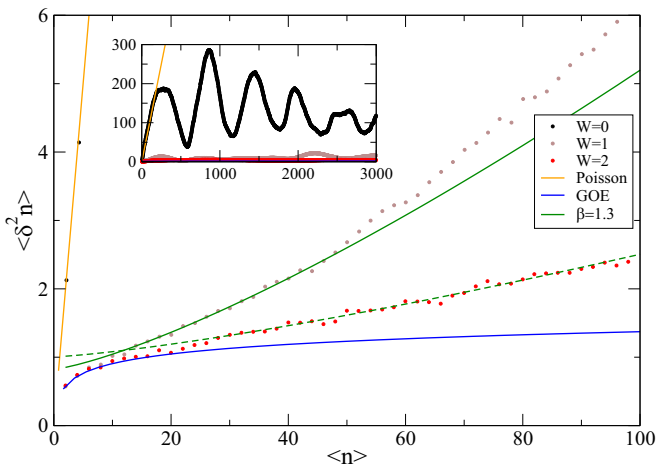
FIG. 10. The number variance $\langle \delta^2 n(E) \rangle$ as a function of $\langle n(E) \rangle$ for weak disorder ($L = 14$; $W = 0$, 1, 2; $P = 4096$; and $M = 4096$). The Poisson and Wigner behaviors correspond to the orange and blue curves correspondingly. The inset presents the whole range of $\langle n(E) \rangle$ values, while the main figure zooms into smaller $\langle n(E) \rangle$. The green curves correspond to $\langle \delta^2 n(E) \rangle \sim \langle n(E) \rangle^\beta$ with $\beta = 1.3$ and the full and dashed line represent different prefactors.

VI. SINGULAR VALUE DECOMPOSITION GLOBAL UNFOLDING

Another way that SVD can be used, is to apply its results for unfolding the spectra and then perform a standard number variance calculation. The unfolding is based on reconstructing the matrix X where the first (or few) contributions of the SV decomposition are dropped since they encode the global behavior. Specifically, capturing the global behavior of the energy spectrum by $\tilde{X}_{lp} = \sum_{k=m}^{r} \sigma_k X_{lp}^{(k)}$ (see Appendix) with m determined by examining the scree plot and identifying the point where the first few modes change the behavior. For example, in the scree plot for the $L = 14$, $W = 2$ case seen in the inset of Fig. 6, one chooses $m = 4$.

Defining the global unfolded lth eigenvalue of the pth realization as

$$\tilde{\varepsilon}_l = \tilde{\varepsilon}_{l-1} + \frac{X_{lp} - X_{l(p-1)}}{\tilde{X}_{lp} - \tilde{X}_{l(p-1)}} + 1, \qquad (3)$$

and calculating the number variance centered on the middle of the unfolded spectra, results in the number variance presented in Fig. 10. Here we focus on the weak disorder regime. First, lets examine the behavior of the number variance for small average numbers, corresponding to small energy scales shown in the main panel. For $W = 0$, we see a close to linear behavior with $\langle \delta^2 n(E) \rangle = \langle n \rangle$. For $W = 1$ and 2, we see see in the inset a Wigner (GOE) behavior, $\langle \delta^2 n(E) \rangle = (2/\pi^2) \ln(\langle n(E) \rangle) + 0.44$, which holds up to $\langle n(E) \rangle \sim 10$ for $W = 1$ and $\langle n(E) \rangle \sim 20$ for $W = 2$.

For large energy scales, a different dependence emerges. The variance saturates with quasiperiodic oscillations which are very pronounced for small disorder and dampened at higher W. This behavior conforms to the low modes (small k) power law seen for λ_k (Fig. 6). In this region $\alpha = 1$, and assuming $\langle \delta^2 n(E) \rangle \sim \langle n(E) \rangle^{\beta = \alpha - 1}$ [93], leading to the expectation that the power-law behavior of the number variance for

large energy scale will correspond to $\beta = 0$, i.e., saturation. Nevertheless, on top of the saturation a quasiperiodic oscillations is observed. This is the result of the finite range of k for which the exponent is equal to 1.

For the weakly disordered regime ($W = 1, 2$) the long time (small energy scales) Wigner behavior is followed by an intermediate time and energy scale for which $\langle \delta^2 n(E) \rangle \sim \langle n(E) \rangle^\beta$, and $\beta = 1.3$ (for $W = 1$ fit to the range $10 < \langle n(E) \rangle < 50$, and for $W = 2$ to $30 < \langle n(E) \rangle < 100$). This corresponds to powers larger than 2 we have seen in the scree plot for the SV amplitudes. Thus this regime corresponds to $E_{\text{Th}} < \langle n(E) \rangle \delta < E_{\text{Ex}}$. The estimation in the previous section (assuming a factor two) for $L = 14$ and $W = 1$ of $E_{\text{Th}} \sim 20\delta$ and $E_{\text{Ex}} \sim 40\delta$, while for $W = 2$, $E_{\text{Th}} \sim 40\delta$, and $E_{\text{Ex}} \sim 100\delta$. These estimations fits reasonably well the range of the super-Poissonian behavior seen for the globally unfolded number variation. Moreover, $\beta = \alpha - 1 = 1.3$ in line with the behavior of the exponent observed for the SV in the region of $k_{\text{Th}} < k < k_{\text{Ex}}$.

VII. DISCUSSION

In the previous sections, it has been shown that the energy spectra of the quantum random antiferromagnetic Ising chain with mixed transverse and longitudinal fields displays a clear signature of a super-Poissonian behavior for a range of energies $E_{\text{Th}} < E < E_{\text{Ex}}$. The super-Poissonian behavior appears deep in the metallic regime and its range grows as the system approaches the MBL transition. On the other hand, the scree plot power law of the energy range $E_{\text{Th}} < E < E_{\text{Ex}}$ approaches two as expected for Poisson as one gets closer to the localized regime. The super-Poissonian behavior becomes more pronounced as the system size increases, and exhibits scaling behavior as a function of the number of realizations and range of eigenvalues considered. Thus the super-Poissonian regime is robust and does not seem to be an artifact of small systems, although it is hard to extrapolate to much larger systems. This behavior is brought to light once global unfolding and sample to sample fluctuations are taken into account using the SVD method, both by scrutinizing the scree plot of the SV amplitudes as well as studying the number variance of the spectra after unfolding the spectra by SVD.

Thus, for a model which is one of the canonical microscopical models for studying the MBL transition, the metallic phase is far from trivial. The small energy scales show all the universal features expected in the metallic regime, while higher energy scales clearly are nonuniversal. A non universal behavior at large energies has also been very recently seen for an other canonical microscopic model for MBL, the Heisenberg chain [94]. Nevertheless, E_{Ex} is not observed there since only a small range of eigenvalues were considered, similar to the $P = 2048$ case depicted in Fig. 8(b). As in itself the deviation from universal behavior of the spectrum at larger energy scales is not surprising, since a somewhat similar deviation from the universal behavior of the energy spectra is seen in the single-particle energy spectrum and associated with the Thouless energy. There the reason for the termination of the universal behavior is very clear. At short times (corresponding to large energy scales) diffusive behavior has not had time to evolved and experience the whole

sample and therefore the behavior is not yet universal. For the Imbrie model the crossover from the short time behavior does not occur directly to the diffusive (universal) behavior, but there is an intermediate times for which the motion of a wave packet is extended, but nevertheless it does not cover the whole phase space and only on longer times it crosses over to the diffusive regime. Both crossovers leave a distinct signature in the energy spectrum and establishes energy scales (E_{Ex} and E_{Th}) which can be extracted using SVD. This regime exists only in the metallic regime, while in the localized regime there is only a transition from nonuniversal short times behavior to a localized behavior.

It would be very interesting to independently study the NEE phase of the Imbrie model by investigating the wavefunction behavior in this regime. Following the methods used in the study of the fractal features of the wave functions of the NEE phase in the GRP model [33–40], one could extended the understanding of the NEE phase in the Imbrie model.

The origin of this intermediate energy (or time) regime is not clarified by this study. Whether is stems from the structure of the coupling of states in the Fock space resulting in a quantum random graph, or other explanations which hinge on static or dynamical rare regions in the system such as Griffiths regions which may drive KT transitions, needs more study. Of course clarifying the finite size scaling of the intermediate regime is highly desirable, but unfortunately seems beyond current and reasonable future numerical capabilities. A possible continuation to this study would be the study of the energy spectrum of other models with a different geometry than the 1D chains, such as the a random network or a modified SYK model. Although one will continue to suffer from the constrains of small systems, one will have freedom of tweaking geometry which may help understanding the physics behind this intermediate region.

APPENDIX: SINGULAR VALUE DECOMPOSITION

The singular value decomposition (SVD) [96–98] is a method to decompose a matrix X of size $M \times P$ (X is not necessarily Hermitian nor square) into a sum of matrices. The matrix X represents data arranged by rows and columns, where the arrangement depends on the application. For the SVD analysis of the spectrum, one writes the M realizations of disorder and the P eigenvalues each, as a matrix X of size $M \times P$, where X_{mp} is the p level of the mth realization. The matrix X is decomposed to $X = U \Sigma V^T$, where U and V are $M \times M$ and $P \times P$ matrices correspondingly, and Σ is a *diagonal* matrix of size $M \times P$ and rank $r = \min(M, P)$. The r diagonal elements of Σ, denoted as σ_k are the singular values (SV) of the matrix which are positive and could be ordered by their size such that $\sigma_1 \geqslant \sigma_2 \geqslant \ldots \sigma_r$. The Hilbert-Schmidt norm of the matrix $||X||_{\mathrm{HS}} = \sqrt{\mathrm{Tr} X^\dagger X} = \sum_k \lambda_k$ (where $\lambda_k = \sigma_k^2$). Therefore using the SVD the matrix X could be written as a series composed of matrices $X^{(k)}$, where $X_{ij}^{(k)} = U_{ik} V_{jk}^T$ and $X_{ij} = \sum_k \sigma_k X_{ij}^{(k)}$. Thus this series in an approximation of matrix X, where the sum of the first m modes gives a matrix $\tilde{X} = \sum_{k=1}^m \sigma_k X^{(k)}$, for which $||X||_{\mathrm{HS}} - ||\tilde{X}||_{\mathrm{HS}}$ is minimal.

[1] I. V. Gornyi, A. D. Mirlin, and D. G. Polyakov, Phys. Rev. Lett. **95**, 206603 (2005).

[2] D. Basko, I. Aleiner, and B. Altshuler, Ann. Phys. (NY) **321**, 1126 (2006).

[3] J. M. Deutsch, Phys. Rev. A **43**, 2046 (1991).

[4] M. Srednicki, Phys. Rev. E **50**, 888 (1994).

[5] V. Oganesyan and D. A. Huse, Phys. Rev. B **75**, 155111 (2007).

[6] A. Pal and D. A. Huse, Phys. Rev. B **82**, 174411 (2010).

[7] D. J. Luitz, N. Laflorencie, and F. Alet, Phys. Rev. B **91**, 081103(R) (2015).

[8] R. Mondaini and M. Rigol, Phys. Rev. A **92**, 041601(R) (2015).

[9] T. Chanda, P. Sierant, and J. Zakrzewski, Phys. Rev. Research **2**, 032045(R) (2020).

[10] F. Monteiro, T. Micklitz, M. Tezuka, and A. Altland, Phys. Rev. Research **3**, 013023 (2021).

[11] M. Schreiber, S. S. Hodgman, P. Bordia, H. P. Lüschen, M. H. Fischer, R. Vosk, E. Altman, U. Schneider, and I. Bloch, Science **349**, 842 (2015).

[12] J.-Y. Choi, S. Hild, J. Zeiher, P. Schauß, A. Rubio-Abadal, T. Yefsah, V. Khemani, D. A. Huse, I. Bloch, and C. Gross, Science **352**, 1547 (2016).

[13] P. Roushan, C. Neill, J. Tangpanitanon, V. M. Bastidas, A. Megrant, R. Barends, Y. Chen, Z. Chen, B. Chiaro, A. Dunsworth *et al.*, Science **358**, 1175 (2017).

[14] K. Xu, J. J. Chen, Y. Zeng, Y. R. Zhang, C. Song, W. Liu, Q. Guo, P. Zhang, D. Xu, H. Deng, K. Huang, H. Wang, X. Zhu, D. Zheng, and H. Fan, Phys. Rev. Lett. **120**, 050507 (2018).

[15] A. Rubio-Abadal, J.-Y. Choi, J. Zeiher, S. Hollerith, J. Rui, I. Bloch, and C. Gross, Phys. Rev. X **9**, 041014 (2019).

[16] D. S. Fisher, Phys. Rev. Lett. **69**, 534 (1992); Phys. Rev. B **51**, 6411 (1995).

[17] For a comprehensive review see: F. Iglói and C. Monthus, Phys. Rep. **412**, 277 (2005); An overview of newer results is given by the sameauthors in: Eur. Phys. J. B **91**, 290 (2018).

[18] P. Lajkó, J.-C. A. d'Auriac, H. Rieger, and F. Iglói, Phys. Rev. B **101**, 024203 (2020).

[19] J. Z. Imbrie, Phys. Rev. Lett. **117**, 027201 (2016).

[20] J. Z. Imbrie, J. Stat. Phys. **163**, 998 (2016).

[21] G. Biroli and M. Tarzia, Phys. Rev. B **102**, 064211 (2020).

[22] M. Tarzia, Phys. Rev. B **102**, 014208 (2020).

[23] D. A. Abanin, J. H. Bardarson, G. De Tomasi, S. Gopalakrishnan, V. Khemani, S. A. Parameswaran, F. Pollmann, A. C. Potter, M. Serbyn, and R. Vasseur, Ann. Phys. **427**, 168415 (2021).

[24] G. De Tomasi, I. M. Khaymovich, F. Pollmann, and S. Warzel, Phys. Rev. B **104**, 024202 (2021).

[25] M. L. Mehta, *Random Matrices*, 2nd ed. (Academic Press, New York, 1991).

[26] B. I. Shklovskii, B. Shapiro, B. R. Sears, P. Lambrianides, and H. B. Shore, Phys. Rev. B **47**, 11487 (1993).

[27] T. Guhr, A. Muller-Groeling, and H. A. Weidenmuller, Phys. Rep. **299**, 190 (1998).

[28] Y. Alhassid, Rev. Mod. Phys. **72**, 895 (2000).

[29] A. D. Mirlin, Phys. Rep. **326**, 259 (2000).

[30] F. Evers and A. D. Mirlin, Rev. Mod. Phys. **80**, 1355 (2008).

[31] B. Altshuler and B. Shklovskii, Zh. Eksp. Teor. Fiz. **91**, 220 (1986) [Sov. Phys. JETP **64**, 127 (1986)].

[32] N. Rosenzweig and C. E. Porter, Phys. Rev. **120**, 1698 (1960).

[33] V. E. Kravtsov, I. M. Khaymovich, E. Cuevas, and M. Amini, New J. Phys. **17**, 122002 (2015).

[34] C. Monthus, J. Phys. A: Math. Theor. **50**, 295101 (2017).

[35] V. Kravtsov, B. Altshuler, and L. Ioffe, Ann. Phys. **389**, 148 (2018).

[36] E. Bogomolny and M. Sieber, Phys. Rev. E **98**, 032139 (2018).

[37] P. A. Nosov, I. M. Khaymovich, and V. E. Kravtsov, Phys. Rev. B **99**, 104203 (2019).

[38] M. Pino, J. Tabanera, and P. Serna, J. Phys. A: Math. Theor. **52**, 475101 (2019).

[39] G. de Tomasi, M. Amini, S. Bera, I. M. Khaymovich, and V. E. Kravtsov, SciPost Phys. **6**, 14 (2019).

[40] I. M. Khaymovich, V. E. Kravtsov, B. L. Altshuler, and L. B. Ioffe, Phys. Rev. Research **2**, 043346 (2020).

[41] R. Berkovits, Phys. Rev. B **102**, 165140 (2020).

[42] A. M. García-García and J. J. M. Verbaarschot, Phys. Rev. D **94**, 126010 (2016).

[43] A. De Luca, B. L. Altshuler, V. E. Kravtsov, and A. Scardicchio, Phys. Rev. Lett. **113**, 046806 (2014).

[44] A. De Luca and A. Scardicchio, Europhys. Lett. **101**, 37003 (2013).

[45] B. L. Altshuler, E. Cuevas, L. B. Ioffe, and V. E. Kravtsov, Phys. Rev. Lett. **117**, 156601 (2016).

[46] K. S. Tikhonov, A. D. Mirlin, and M. A. Skvortsov, Phys. Rev. B **94**, 220203(R) (2016).

[47] M. Pino, L. B. Ioffe, and B. L. Altshuler, Proc. Natl. Acad. Sci. USA **113**, 536 (2016).

[48] M. Pino, V. E. Kravtsov, B. L. Altshuler, and L. B. Ioffe, Phys. Rev. B **96**, 214205 (2017).

[49] E. J. Torres-Herrera and L. F. Santos, Ann. Phys. **529**, 1600284 (2017).

[50] G. Biroli and M. Tarzia, arXiv:1810.07545.

[51] K. S. Tikhonov and A. D. Mirlin, Phys. Rev. B **99**, 024202 (2019).

[52] K. S. Tikhonov and A. D. Mirlin, Phys. Rev. B **99**, 214202 (2019).

[53] L. Faoro, M. Feigel'man, and L. Ioffe, Ann. Phys. (NY) **409**, 167916 (2019).

[54] K. Kechedzhi, V. Smelyanskiy, J. R. McClean, V. S. Denchev, M. Mohseni, S. Isakov, S. Boixo, B. Altshuler, and H. Neven, Phys. Rev. X **10**, 011017 (2020).

[55] Y. Bar Lev, G. Cohen, and D. R. Reichman, Phys. Rev. Lett. **114**, 100601 (2015).

[56] K. Agarwal, S. Gopalakrishnan, M. Knap, M. Müller, and E. Demler, Phys. Rev. Lett. **114**, 160401 (2015).

[57] E. J. Torres-Herrera and L. F. Santos, Phys. Rev. B **92**, 014208 (2015).

[58] D. J. Luitz, N. Laflorencie, and F. Alet, Phys. Rev. B **93**, 060201(R) (2016).

[59] D. J. Luitz and Y. Bar Lev, Phys. Rev. Lett. **117**, 170404 (2016).

[60] D. J. Luitz and Y. Bar Lev, Ann. Phys. **529**, 1600350 (2017).

[61] K. Agarwal, E. Altman, E. Demler, S. Gopalakrishnan, D. A. Huse, and M. Knap, Ann. Phys. **529**, 1600326 (2017).

[62] S. Bera, G. De Tomasi, F. Weiner, and F. Evers, Phys. Rev. Lett. **118**, 196801 (2017).

[63] E. V. H. Doggen, F. Schindler, K. S. Tikhonov, A. D. Mirlin, T. Neupert, D. G. Polyakov, and I. V. Gornyi, Phys. Rev. B **98**, 174202 (2018).

[64] H. P. Lüschen, P. Bordia, S. Scherg, F. Alet, E. Altman, U. Schneider, and I. Bloch, Phys. Rev. Lett. **119**, 260401 (2017).

[65] P. Bordia, H. P. Lüschen, S. Scherg, S. Gopalakrishnan, M. Knap, U. Schneider, and I. Bloch, Phys. Rev. X **7**, 041047 (2017).

[66] B. L. Altshuler, Y. Gefen, A. Kamenev, and L. S. Levitov, Phys. Rev. Lett. **78**, 2803 (1997).

[67] S. Gopalakrishnan, M. Muller, V. Khemani, M. Knap, E. Demler, and D. A. Huse, Phys. Rev. B **92**, 104202 (2015).

[68] R. Vosk, D. A. Huse, and E. Altman, Phys. Rev. X **5**, 031032 (2015).

[69] A. C. Potter, R. Vasseur, and S. A. Parameswaran, Phys. Rev. X **5**, 031033 (2015).

[70] L. Zhang, B. Zhao, T. Devakul, and D. A. Huse, Phys. Rev. B **93**, 224201 (2016).

[71] S. Gopalakrishnan, K. Agarwal, E. A. Demler, D. A. Huse, and M. Knap, Phys. Rev. B **93**, 134206 (2016).

[72] R. Berkovits, Phys. Rev. B **97**, 115408 (2018).

[73] Y. Bar Lev and D. R. Reichman, Euro. Phys. Lett. **113**, 4600 (2016).

[74] E. V. H. Doggen, I. V. Gornyi, A. D. Mirlin, and D. G. Polyakov, Phys. Rev. Lett. **125**, 155701 (2020).

[75] O. Motrunich, S.-C. Mau, D. A. Huse, and D. S. Fisher, Phys. Rev. B **61**, 1160 (2000).

[76] I. A. Kovács and F. Iglói, Phys. Rev. B **82**, 054437 (2010).

[77] F. Thompson and R. R. P. Singh, Phys. Rev. E **99**, 032129 (2019).

[78] Y. Liu, S. Qi, J. Fang, J. Sun, C. Liu, Y. Liu, J. Qi, Y. Xing, H. Liu, X. Lin, L. Wang, Q.-K. Xue, X. C. Xie, and J. Wang, Phys. Rev. Lett. **127**, 137001 (2021).

[79] T. Thiery, F. Huveneers, M. Müller, and W. De Roeck, Phys. Rev. Lett. **121**, 140601 (2018).

[80] A. Goremykina, R. Vasseur, and M. Serbyn, Phys. Rev. Lett. **122**, 040601 (2019).

[81] P. T. Dumitrescu, A. Goremykina, S. A. Parameswaran, M. Serbyn, and R. Vasseur, Phys. Rev. B **99**, 094205 (2019).

[82] A. Morningstar and D. A. Huse, Phys. Rev. B **99**, 224205 (2019).

[83] A. Morningstar, D. A. Huse, and J. Z. Imbrie, Phys. Rev. B **102**, 125134 (2020).

[84] D. Braun and G. Montambaux, Phys. Rev. B **52**, 13903 (1995).

[85] E. Cuevas, E. Louis, M. Ortuño, and J. A. Vergés, Phys. Rev. B **56**, 15853 (1997).

[86] A. M. García-García, Y. Jia, and J. J. M. Verbaarschot, Phys. Rev. D **97**, 106003 (2018).

[87] C. L. Bertrand and A. M. García-García, Phys. Rev. B **94**, 144201 (2016).

[88] Á. L. Corps, R. A. Molina, and A. Relaño, Phys. Rev. B **102**, 014201 (2020).

[89] Y. Wang, C. Cheng, X.-J. Liu, and D. Yu, Phys. Rev. Lett. **126**, 080602 (2021).

[90] R. Fossion, G. Torres Vargas, and J. C. López Vieyra, Phys. Rev. E **88**, 060902(R) (2013).

[91] G. Torres-Vargas, R. Fossion, C. Tapia-Ignacio, and J. C. López-Vieyra, Phys. Rev. E **96**, 012110 (2017).

[92] G. Torres-Vargas, J. A. Méndez-Bermúdez, J. C. López Vieyra, and R. Fossion, Phys. Rev. E **98**, 022110 (2018).

[93] R. Berkovits, Phys. Rev. B **104**, 054207 (2021).

[94] W.-J. Rao, Phys. Rev. B **105**, 054207 (2022).

[95] Y. Y. Atas, E. Bogomolny, O. Giraud, and G. Roux, Phys. Rev. Lett. **110**, 084101 (2013).

[96] C. D. Martin and M. A. Porter, Am. Math. Month. **119**, 838 (2012).

[97] M. L. Fowler, M. Chen, J. A. Johnson, and Z. Zhou, Signal Process. **90**, 2190 (2010).

[98] H. R. Swathi, S. Sohini, Surbhi, and G. Gopichand, IOP Conf. Ser.: Mater. Sci. Eng. **263**, 042082 (2017).